Dynamic realization of statistical state in finite systems

Xizhen Wu,[1] Fumihiko Sakata,[2] Yizhong Zhuo,[1,3] Zhuxia Li,[1] and Nguyen Dinh Dang[2,*]
[1]*China Institute of Atomic Energy, P.O. Box 275(18), Beijing, People's Republic of China*
[2]*Institute for Nuclear Study, University of Tokyo, Tanashi, Tokyo 188, Japan*
[3]*Institute of Theoretical Physics, Academia Sinica, Beijing 100080, People's Republic of China*
(Received 7 August 1995)

Evolution of the large-amplitude dissipative collective motion in a simple soluble model is studied within the time-dependent Hartree-Fock theory, by using a general microscopic transport theory, which optimally divides the total system into the collective and intrinsic subsystems. Even though the total system reaches some statistical stationary state, it is shown that the subsystem cannot alone remain stationary by being separated from the other subsystem, when they are strongly correlated with each other. Dynamic response functions are used in exploring an instantaneous structure of each subsystem. When the total system reaches a statistical stationary state, it is shown by using the dynamical response function that the influence of the intrinsic subsystem on the collective one can be effectively taken into account by replacing the intrinsic system by the heat bath.

PACS number(s): 24.60.Ky, 03.65.Sq, 21.10.Re, 21.60.Jz

I. INTRODUCTION

One of the basic problems in the nuclear physics is to microscopically understand phenomena such as damping, dissipation, fluctuation, and diffusion processes, which appear in the giant resonance of hot nuclei, fission, fusion, heavy-ion deep-inelastic collisions, etc. They involve a complex interplay between the collective and intrinsic degrees of freedom, the latter one usually expressed by a statistical object like the thermal heat bath or the Gaussian orthogonal ensemble (GOE). In such a finite many-body system as the nucleus, however, the Born-Oppenheimer approximation to divide the total system into the collective and intrinsic subsystems is by no means trivial, nor is the statistical assumption.

Since we are interested in the large-amplitude dissipative collective motion whose energy is much smaller than the Fermi energy of the single-particle motion, its microscopic dynamics ought to be studied within the time-dependent Hartree-Fock (TDHF) theory. As is well known, the TDHF equation is formally equivalent to the Hamilton canonical equations of motion within the TDHF symplectic manifold. Therefore, the study of nuclear dissipative dynamics has a large overlap with the celebrated ergodic problem which provides us with the dynamical foundation of classical statistical mechanics [1,2]. In the case of the ergodic problem, one treats a long time evolution of the single trajectory and discusses a relation between the phase-space average and the time average. In the case of nuclear physics, one may deal with a time development of a bundle of TDHF trajectories. It approximately represents a wave packet consisting of many eigenfunctions which are expressed by the direct product of intrinsic and collective components. When one treats a dissipative collective motion, these eigenfunctions at the initial time are supposed to have a different structure for the intrinsic component, whereas they have almost the same structure for the collective component. To investigate the dynamical evolution process of the bundle of trajectories, one has to answer the following important questions: (a) a relation between the dynamics of individual trajectories and that of the bundle of trajectories, (b) how and why the system described by the bundle of trajectories reaches its stationary state, and what the final state looks like, (c) the dynamical relation between two subsystems which are composed of the collective and the intrinsic degrees of freedom, respectively, namely, how the collective subsystem is affected by its partner during the evolution process in a strongly interacting finite system, and (d) how to macroscopically describe the evolutional process of the bundle of trajectory. In other words, how to microscopically derive a Fokker-Planck- or Langevin-type transport equation for the collective degrees of freedom.

These investigations involve a vast number of theoretical subjects. In the realistic case, an initial wave packet is composed of many different intrinsic excitations with almost the same collective component. Even in this specific problem, a later-on time evolution may show quite a different development depending on its initial condition. In this paper, we will concentrate our discussion on how a statistical state in the finite system is realized dynamically.

The general microscopic transport theory [3–6] has been proposed to describe the collective motion displayed by the bundle of trajectories. In this theory, the total system is optimally divided into the collective and intrinsic subsystems, and the dynamic response and correlation functions have been introduced [5] for studying the evolution process of the bundle of trajectories. By applying the theory to a simple model Hamiltonian in the previous paper [5], it was illustrated that the *dynamic response function* gives important information in understanding the dynamical process of the total system as well as the subsystems. In the present paper, we further analyze the later-on time evolution of the bundle of trajectories by using this general theory.

*Permanent address: Institute of Nuclear Science and Technique, Vietnam Atomic Energy Commission, 67 Nguyen Du, Hanoi, Vietnam.

Using a simple model Hamiltonian, in Sec. II, we discuss the importance of analyzing the structure of the TDHF manifold, which gives full information of the individual trajectories. In Sec. III, we explore the evolution process of the bundle of trajectories. By performing numerical calculations, we found an important condition where the total system resists being divided into two subsystems. Namely, we found a condition for characterizing the specific situation where the total system converges to some (statistical) stationary state, whereas the subsystem cannot alone stay in the stationary state without its partner.

We also found that the dynamic response functions for the subsystems show quite different behavior from that of the usual linear response function [7,8]. When the total system reaches a statistical stationary state, it is shown in Sec. IV by using the dynamical response function that the intrinsic subsystem is effectively expressed by a heat bath. Since the response function is directly related to experimental observables, all of these findings will certainly provide us with further insight into the statistical description of large-amplitude dissipative collective motion in finite systems.

II. MODEL HAMILTONIAN AND STRUCTURE OF THE TDHF MANIFOLD

In understanding the large-amplitude dissipative collective motion, the importance of mutual dependence between the collective and the single-particle motion has been pointed out repeatedly. One of the main issues in this respect has been to make clear whether the single-particle motion develops along the adiabatic basis or the diabatic one, which are defined by referring to the time-dependent variation of the mean field induced by the collective motion. This problem has been usually discussed to describe the dynamical evolution of the collective motion near the level-crossing region [9–11]. Since the adiabatic assumption is strongly violated near the level-crossing point, the dynamical evolution of the system cannot be expressed by the adiabatic collective variables alone or the diabatic path. In this case one faces a dynamical problem as to how many additional degrees of freedom are necessary in describing the collective motion besides the collective variables.

In order to understand the microscopic dynamics responsible for the dissipation process by going beyond the adiabatic assumption, therefore, it is indispensable to explore the structure of the TDHF manifold, which determines what kinds of dynamics can occur in the finite system. Until quite recently, it was not well recognized in nuclear physics that there is exceedingly rich structure in the TDHF manifold, which is not simply expected from the shape of the potential energy surface. In order to find various modes of motions appearing in the TDHF manifold, one has to numerically solve the TDHF equation with different initial conditions.

To get a fully microscopic understanding of the complex structure of the classical phase space, there has been developed the general theory of nonlinear dynamics (GTND) [2]. The basic ideas of the GTND have been mainly developed by using the classical system with 2 degrees of freedom or even 1.5 degrees of freedom like the kicked rotor model. Since our main concern is to explore the justification of an introduction of some statistical treatment in the finite system through what is happening during the time evolution of a bundle of trajectories, we study the relation between the characteristic features of the individual trajectories and those of the bundle of trajectories in the TDHF manifold. For this aim, we take the following system with two degrees of freedom:

$$H(q_1,p_1;q_2,p_2)=H_1+H_2+H_{\rm coupl},$$

$$H_i=\frac{1}{2}\varepsilon_i(q_i^2+p_i^2)+\frac{1}{2}V_i(N-1)(q_i^2-p_i^2)-\frac{N-1}{N}\frac{V_i}{4}(q_i^4-p_i^4),\quad i=1,2,$$

$$H_{\rm coupl}=\sum_i A^iB^i,$$

$$A^i=\sqrt{\frac{V_i(1-N)}{4N}}[q_1^2+(-1)^ip_1^2],\quad B^i=\sqrt{\frac{V_i(1-N)}{4N}}[q_2^2+(-1)^ip_2^2]. \tag{2.1}$$

The above Hamiltonian is a classical realization of the quantum mechanical SU(3) Hamiltonian for the many-fermion system by applying the TDHF formalism (the convention $\hbar=1$ is applied). The structure of the TDHF manifold (which is formally equivalent to the classical phase space) is numerically obtained by solving the canonical equations of motion given by

$$\dot{q}_i=\frac{\partial H}{\partial p_i},\quad \dot{p}_i=-\frac{\partial H}{\partial q_i}. \tag{2.2}$$

In Fig. 1, the Poincaré section map constructed on the (q_1,p_1) plane with conditions $q_2=0$ and $p_2>0$ is shown. The parameters used in our calculation are $\varepsilon_0=0$, $\varepsilon_1=1$, $\varepsilon_2=2$, and $N=30$, and the total energy is fixed at $E=40$. From Fig. 1, one may learn how many rich structures are there in the TDHF manifold depending on the interaction strength V_i. In Fig. 1, the essential phenomena discussed in the GTND are clearly displayed. The objective of the GTND has been to understand how the adiabatic invariants (constants of motion) characterizing the individual trajectories undergo a change depending on their amplitudes at the origin

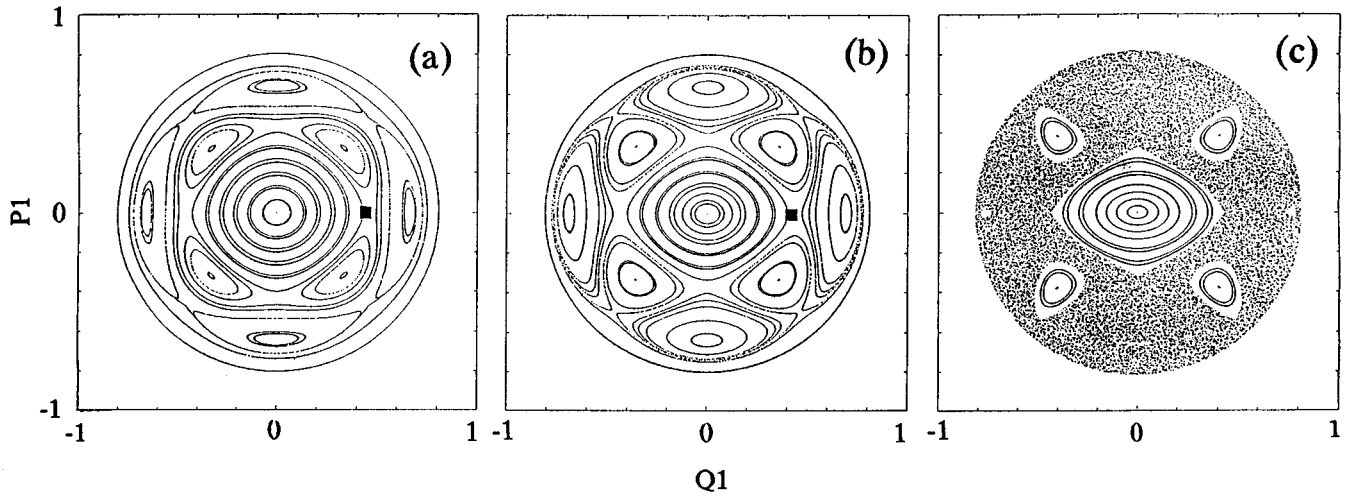

FIG. 1. Poincaré section map on the (q_1,p_1) plane. (a), (b), and (c) are for $V=-0.01,-0.03$, and -0.07, respectively.

of the coordinate system, how there appears a new type of motion forming a resonant island structure which surrounds the main island, how and why the local adiabatic invariant characterizing the motion belonging to the resonant islands disappears (appearance of local chaoticity), and how there finally appears the global chaoticity. To get an analytical understanding of these phenomena, it turns out to be decisive to introduce the *most natural coordinate system* for each trajectory. It may not be an exaggeration to say that the history of the nonlinear dynamics has been the struggle to develop a proper classical perturbation theory capable of defining the most optimum coordinate system, where an approximate adiabatic invariant of a given trajectory is expressed in the simplest way. In the nuclear physics, this problem is equivalent to developing a method which optimally divides the total system into the collective and intrinsic degrees of freedom.

Here it should be noticed that the Hamiltonian in Eq. (2.1) satisfies the relations

$$\left.\frac{\partial H}{\partial q_2}\right|_{p_2=q_2=0}=\left.\frac{\partial H}{\partial p_2}\right|_{p_2=q_2=0}=0,$$
$$\left.\frac{\partial H}{\partial q_1}\right|_{p_1=q_1=0}=\left.\frac{\partial H}{\partial p_1}\right|_{p_1=q_1=0}=0, \tag{2.3}$$

which are called the *maximal decoupling conditions*. Equations (2.3) simply mean that the trajectory starting with the initial condition $q_1(t=0)=q_{10}$, $p_1(t=0)=p_{10}$, $q_2(t=0)=0$, $p_2(t=0)=0$ is always running on the subspace Σ_1 $\{q_1,p_1;q_2=0,p_2=0\}$, whereas the trajectory with the initial condition $q_1(t=0)=0$, $p_1(t=0)=0$, $q_2(t=0)=q_{20}$, $p_2(t=0)=p_{20}$ is always on the subspace Σ_2 $\{q_1=0,p_1=0;q_2,p_2\}$. In this sense, the coordinate system $\{q_1,p_1;q_2,p_2\}$ satisfying the conditions (2.3) gives the most optimal coordinate system for the trajectories which are sticking to either the subspace Σ_1 or to Σ_2. In other words, the division of the total system into the *relevant coordinates* $\{q_1,p_1\}$ and the *irrelevant coordinates* $\{q_2,p_2\}$ has a sense in a region near these subspaces. In Fig. 1, the trajectories sticking to the subspace Σ_2 form an innermost concentric circle structure centered at the origin, whereas those sticking to the subspace Σ_1 form an outermost concentric circle structure. Trajectories starting far away from both the subspaces Σ_1 and Σ_2 show a crescent structure in Fig. 1(a). In this case, the coordinate system $\{q_1,p_1;q_2,p_2\}$ has no advantage, because their adiabatic invariants cannot be simply expressed by either one of these two. As is seen from Fig. 1, in the cases with $V_i=-0.01$ and -0.03, these trajectories still represent *regular* motion, forming an island structure surrounding the main island. For these trajectories, one may introduce another most natural coordinate system called the *resonant coordinates* characterized by the nonlinear resonance [2,13].

Trajectories having different adiabatic invariants are separated by the separatrix. As the nonlinear interaction becomes large, it is well known that the chaotic motion starts to occur near the separatrix. In the case with $V_i=-0.07$, the trajectories starting far from the subspace Σ_2 mainly represent the *chaotic* motion. Since there are no constants of motion for the chaotic trajectory, there does not exist any optimal coordinate system.

As is stated in the Introduction, large-amplitude dissipative collective motion can be explored by a time evolution of a bundle of trajectories within the TDHF theory. The time evolution of a bundle initially distributed near the subspace Σ_1 was studied extensively in Ref. [12]. In this paper, we restrict ourselves to the case where a bundle is initially located far away from the subspaces Σ_1 and Σ_2 with a sharp distribution.

III. COUPLED-MASTER EQUATION

A. Evolution of bundle

The time evolution of a bundle of trajectories is described by the Liouville equation given by

$$\dot{\rho}(t)=-i\mathscr{L}\rho(t),\quad \mathscr{L}\equiv\sum_{i=1}^{2}\left(\frac{\partial H}{\partial q_i}\frac{\partial}{\partial p_i}-\frac{\partial H}{\partial p_i}\frac{\partial}{\partial q_i}\right). \tag{3.1}$$

The dynamical relation between the two degrees of freedom is studied by introducing a pair of partial distribution functions

$$\rho_1(t)\equiv\int\int dq_2dp_2\rho(t)=\mathrm{Tr}_2\rho(t),\quad \rho_2(t)\equiv\int\int dq_1dp_1\rho(t)=\mathrm{Tr}_1\rho(t). \tag{3.2}$$

With the aid of the partial distribution functions defined in Eq. (3.2), one may introduce the time-dependent projection operator [14]

$$P(t)\equiv\rho_1(t)\mathrm{Tr}_1+\rho_2(t)\mathrm{Tr}_2-\rho_1(t)\rho_2(t)\mathrm{Tr}_1\mathrm{Tr}_2. \tag{3.3}$$

Then the total distribution function $\rho(t)$ is divided into a separable part $\rho_s(t)$ and a correlation part $\rho_c(t)$ defined through

$$\rho_s(t)\equiv P(t)\rho(t)=\rho_1(t)\rho_2(t),\quad \rho_c(t)\equiv\{1-P(t)\}\rho(t)=\rho(t)-\rho_1(t)\rho_2(t). \tag{3.4}$$

By means of the distribution functions defined in Eqs. (3.2) and (3.4), the coupling Hamiltonian in Eq. (2.1) is expressed as

$$H_{\mathrm{coupl}}=H_{\mathrm{aver}}(t)+H_\Delta(t)-E_0(t), \tag{3.5}$$

$$H_{\mathrm{aver}}(t)\equiv H_1(t)+H_2(t),$$

$$H_\Delta(t)\equiv H_{\mathrm{coupl}}-H_{\mathrm{aver}}(t)+E_0(t)=\sum_{i=1}^{2}(A^i-\langle A^i\rangle_t)(B^i-\langle B^i\rangle_t),$$

$$E_0(t)\equiv\int\int dp_1dq_1dp_2dq_2H_{\mathrm{coupl}}\rho_1(t)\rho_2(t)=\sum_{i=1}^{2}\langle A^i\rangle_t\langle B^i\rangle_t,$$

$$H_1(t)\equiv\int\int dp_2dq_2H_{\mathrm{coupl}}\rho_2(t)=\sum_i A^i\langle B^i\rangle_t,$$

$$H_2(t)\equiv\int\int dp_1dq_1H_{\mathrm{coupl}}\rho_1(t)=\sum_i\langle A^i\rangle_tB^i,$$

$$\langle A^i\rangle_t\equiv\int dq_1dp_1A^i\rho_1(t),\quad \langle B^i\rangle_t\equiv\int dq_2dp_2B^i\rho_2(t), \tag{3.6}$$

where $H_1(t)$ $[H_2(t)]$ denotes a time-dependent Hamiltonian for the first [second] degree of freedom obtained from H_{coupl} by averaging over the second [first] distribution function. The total Hamiltonian is then represented as

$$H=H_{1,\mathrm{mean}}(t)+H_{2,\mathrm{mean}}(t)+H_\Delta(t)-E_0(t), \tag{3.7}$$

$$H_{1,\mathrm{mean}}(t)=H_1+H_1(t),\quad H_{2,\mathrm{mean}}(t)=H_2+H_2(t), \tag{3.8}$$

where $H_{1,\mathrm{mean}}(t)$ $[H_{2,\mathrm{mean}}(t)]$ represents the so-called ''mean-field'' Hamiltonian for the first [second] degree of freedom, which is obtained by only taking account of an average effect of the second [first] degree of freedom. Here $H_\Delta(t)$ is the dynamic fluctuation part.

In performing the numerical calculation, the time evolution of the distribution function $\rho(t)$ organized by Eq. (3.1) is evaluated by using the pseudoparticle method,

$$\rho(t)=\frac{1}{N_p}\sum_{n=1}^{N_p}\prod_{i=1}^{2}\delta(q_i-q_{i,n}(t))\delta(p_i-p_{i,n}(t)), \tag{3.9}$$

where N_p means the total number of pseudoparticles and $q_{i,n}(t)$ and $p_{i,n}(t)$ denote a phase space point of the nth pseudoparticle at time t, which is determined by integrating Eq. (2.2). We use the fourth order Runge-Kutta method for integrating the canonical equation of motion and N_p is chosen to be 10 000. The initial condition of the distribution function is given by a uniform distribution in a region

$$-0.05\leqslant q_1-0.4\leqslant 0.05,\quad -0.02\leqslant q_2-q_{20}\leqslant 0.02,$$

$$-0.05\leqslant p_1\leqslant 0.05,\quad -0.02\leqslant p_2\leqslant 0.02, \tag{3.10}$$

where q_{20} is fixed from the Hamiltonian in Eq. (2.2) by using $q_1=0.4$, $p_1=p_2=0$, and $E=40$. By comparing the above initial condition with the Poincaré map in Fig. 1, it is easily seen that the initial distribution function $\rho(t=0)$ is set in a tiny region near the unstable fixed point, i.e., an intersection point of the separatrix for the first two cases. This choice of initial condition is very interesting because the chaotic feature is known to be first generated near this hyperbolic fixed point. The initial distribution is indicated in Fig. 1 by a solid square.

In Fig. 2(a), the time dependence of the variance $\langle q_1^2\rangle_t - \langle q_1\rangle_t^2$ is shown for the cases with $V_i = -0.01$, -0.03, -0.04, and -0.07. A unit of time is given by $\tau_{\rm coll} = \omega_{\rm coll}/2\pi$, where $\omega_{\rm coll}$ is the eigenfrequency of low-lying normal mode obtained by applying the random phase approximation (RPA) to Eq. (2.2).

As is seen from Fig. 1, every part of the phase space in the cases with $V_i = -0.01$ and -0.03 is dominated by regular motion, but by the chaotic sea in the case with $V_i = -0.07$. In the case with $V_i = -0.01$, the variance is oscillating and even increasing. Since the variance has no tendency to reach some time-independent value, the system is not expected to converge to some statistical object in this case. In the case with a much stronger interaction, i.e., $V_i = -0.03$ and -0.04, the variance increases exponentially and seems to oscillate around some saturation value. Nevertheless, the amplitude of oscillation is not small, indicating the nonestablishment of a stationary state for a very long time. Note that the above result is obtained by choosing an initial distribution around the unstable fixed point where many trajectories with different characters come across each other. If one puts many pseudoparticles around the hyperbolic point where various types of trajectories are involved, the existence of the invariant (KAM) torus prevents the system from reaching some statistical object. Consequently, one cannot expect a realization of the statistical state for the nonlinear dynamical system where the KAM torus is dominating.

In the case with $V_i = -0.07$, where the chaotic sea dominates the phase space, a quite different situation is realized. In the beginning, the variance increases abruptly, steeper than exponential curve which is realized in $V_i = -0.03$ and -0.04. In this case, moreover, the time dependence almost dies out around $t \cong 25\tau_{\rm coll}$, indicating the establishment of the stationary state. Thus the appearance of chaotic motion for the individual trajectory is strongly related to the realization of a stationary state for the bundle of trajectories.

As stated in the previous section, the choice of the coordinate system does not have any sense in the present chaotic case. Namely, if the relations

$$\langle q_i\rangle_t \leqslant \sqrt{\langle q_i^2\rangle_t - \langle q_i\rangle_t^2}, \qquad \langle p_i\rangle_t \leqslant \sqrt{\langle p_i^2\rangle_t - \langle p_i\rangle_t^2} \tag{3.11}$$

hold, the coordinate system $\{q_1, p_1; q_2, p_2\}$ has no particular advantage in describing the system under consideration. In Fig. 2(b), the average value of $\langle p_2\rangle_t$ and the variance $\langle p_2^2\rangle_t - \langle p_2\rangle_t^2$ are shown for the case with $V_i = -0.07$. Since the square root of the variance is much larger than the average, the choice of a paticular coordinate system does not have any profit for the present case. As is well known, the nearest-neighbor level-spacing statistics of the quantum system is well described by the GOE, when the phase space of its classical correspondent is covered by the chaotic sea [15]. Here, it should be noticed that the chaotic phase space structure is generated by a single trajectory, whereas the nearest-neighbor level spacing expresses a statistical property of many eigenstates. Since the GOE is derived under the assumption that the final result should not depend on the choice of representation, and since the time-independent stationary state realized after $t \cong 25\tau_{\rm coll}$ does not depend on the choice of the coordinate system either, we may draw the conclusion that the bundle of trajectories reaches a statistical object after $t \cong 25\tau_{\rm coll}$.

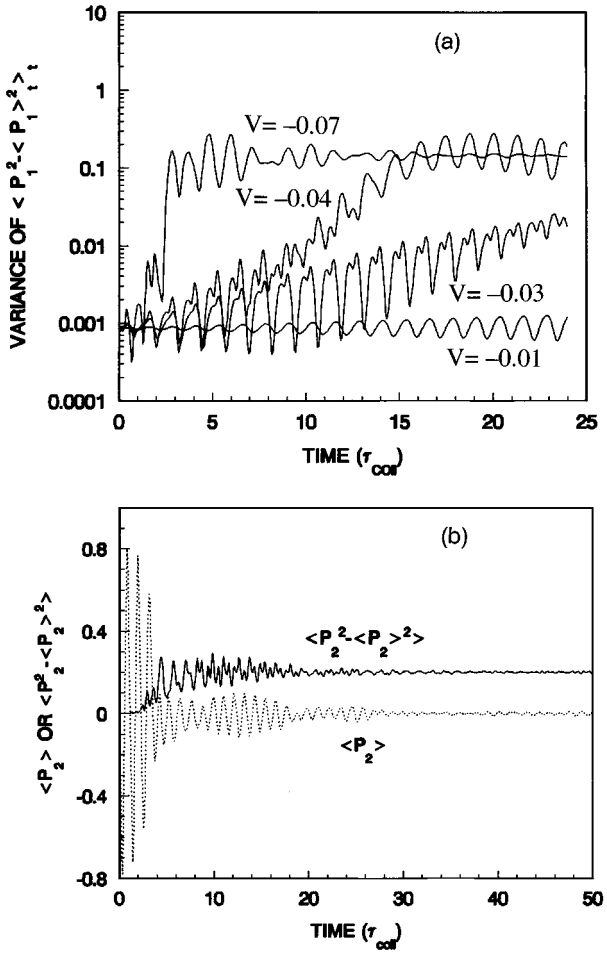

FIG. 2. (a) Time-dependent variance $\langle p_1^2 - \langle p_1\rangle_t^2\rangle_t$ for the cases with $V = -0.01, -0.03, -0.04$, and -0.07. (b) Averaged value $\langle p_2\rangle$ and variance $\langle p_2^2 - \langle p_2\rangle_t^2\rangle_t$ as a function of time for $V = -0.07$.

B. Energy distribution

From the saturation property of the variance depicted in Fig. 2, it is expected that the stationary statistical state is established dynamically for the chaotic case with $V_i = -0.07$. It is the aim of the present subsection to investigate what kind of final distribution is established for the case with $V_i = -0.07$ and how two subsystems described by $\rho_1(t)$ and $\rho_2(t)$ are correlated with each other. Since the energy of each pseudoparticle is chosen to be $E = 40$ in the initial condition, there are no fluctuations in the total Hamiltonian H; i.e., $\langle H^2\rangle_t - \langle H\rangle_t^2 = 0$ at any time.

Now, let us consider the distribution of the partial Hamiltonian. In Figs. 3(a) and 3(b), the time-dependent averages defined through

$$\langle H_i\rangle_t = \int\int dq_i dp_i H_i \rho_i(t), \quad i = 1 \text{ and } 2,$$

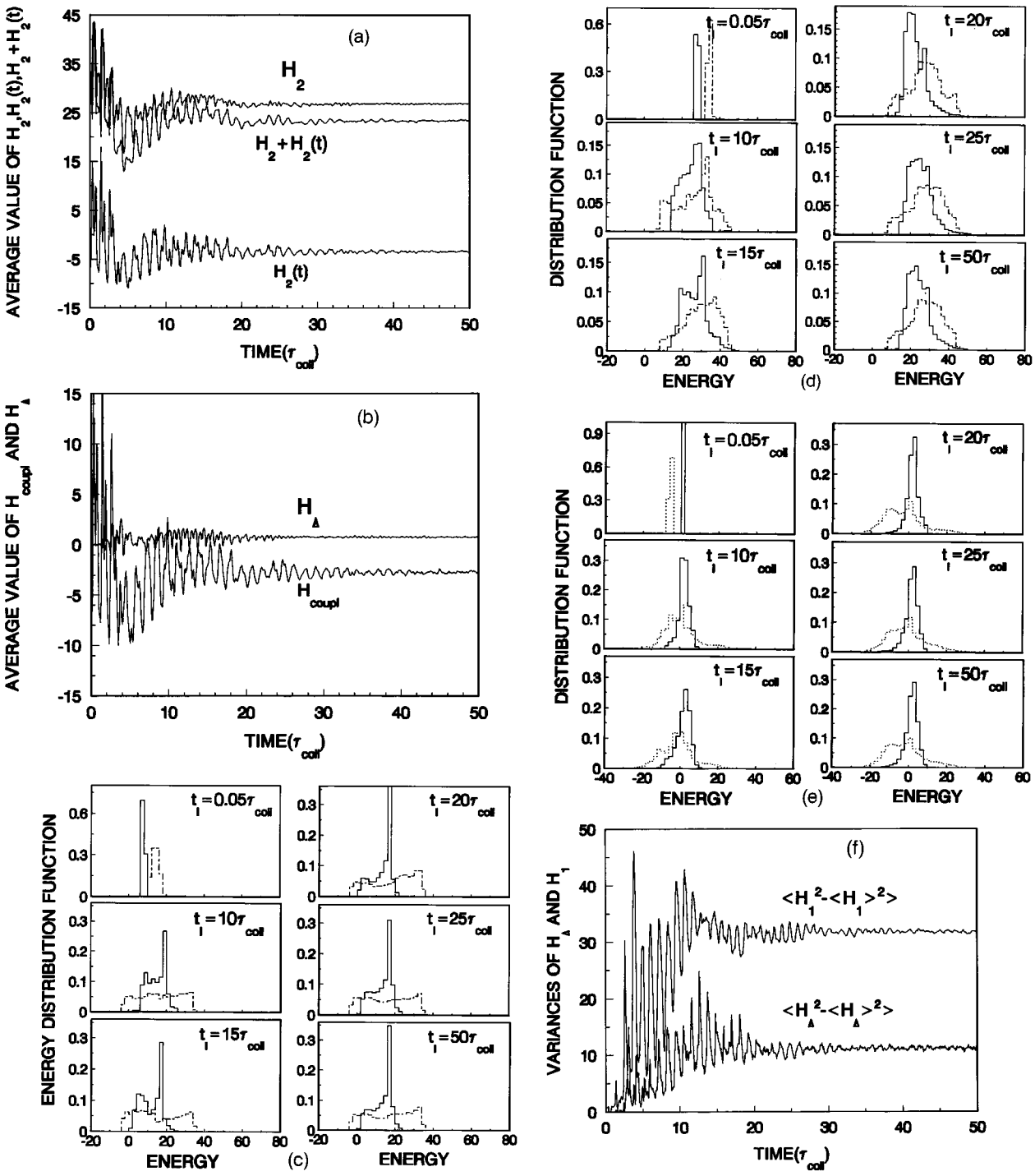

FIG. 3. (a) Time dependence of averaged values $\langle H_2\rangle_t$, $\langle H_2(t)\rangle_t$, and $\langle H_2+H_2(t)\rangle_t$, (b) time dependence of averaged values $\langle H_\Delta(t)\rangle_t$ and $\langle H_{\rm coupl}\rangle_t$, (c) energy distribution of H_1 (dashed line) and $H_1+H_1(t)$ (solid line) for different times t_I, (d) energy distribution of H_2 (dashed line) and $H_2+H_2(t)$ (solid line) for different times t_I, (e) energy distribution of $H_{\rm coupl}$ (dashed line) and H_Δ (solid line) for different times t_I, (f) time-dependent variance $\langle H_\Delta^2-\langle H_\Delta\rangle_t^2\rangle_t$ and $\langle H_1^2-\langle H_1\rangle_t^2\rangle_t$, for the case with $V=-0.07$.

$$\langle H_i+H_i(t)\rangle_t=\int\int dq_i dp_i\{H_i+H_i(t)\}\rho_i(t), \qquad i=1 \text{ and } 2,$$

$$\langle H_{\rm coupl}\rangle_t=\int\int dp_1 dq_1 dp_2 dq_2 H_{\rm coupl}\rho(t)=E_0(t), \qquad \langle H_\Delta(t)\rangle_t=\int\int dp_1 dq_1 dp_2 dq_2 H_\Delta(t)\rho(t)=0 \tag{3.12}$$

are shown. $\langle H_1\rangle_t$, $\langle H_1(t)\rangle_t$, and $\langle H_1+H_1(t)\rangle_t$ are not shown in Fig. 3, but have similar behavior with $\langle H_2\rangle_t$, $\langle H_2(t)\rangle_t$, and $\langle H_2+H_2(t)\rangle_t$. These averages reach their stationary values at $t\cong(25-30)\tau_{\rm coll}$, after a violent exchange

of energy in the region of $t<5\tau_{\rm coll}$. Note that $\langle H_1(t)\rangle_t$, $\langle H_2(t)\rangle_t$, and $\langle H_{\rm coupl}\rangle_t$ are equivalent to $E_0(t)$ by definition. This convergence property is consistent with the saturation property of the variance in Figs. 2(a) and 2(b) discussed in the previous subsection.

A convergence of these average values does not necessarily indicate the establishment of the statistical state for each subsystem. To make this point clear, let us notice that a general relation for various variances of partial Hamiltonians always holds,

$$\Gamma_2^{(i)}\geqslant\Gamma_1^{(j)}\geqslant\Gamma_0(=0),\quad i,j=1 \text{ and } 2,$$
$$\Gamma_0\equiv\langle H^2\rangle-\langle H\rangle^2,$$
$$\Gamma_1^{(i)}\equiv\langle H_{i,\rm mean}^2(t)\rangle-\langle H_{i,\rm mean}(t)\rangle^2,$$
$$\Gamma_2^{(i)}\equiv\langle H_i^2\rangle-\langle H_i\rangle^2, \tag{3.13}$$

which is easily proven. When the mean-field approximation gives a reasonable description, the relation $\Gamma_0\cong\Gamma_1^{(i)}$ holds. When the coupling interaction is sufficiently small, the other relation is also satisfied, i.e., $\Gamma_1^{(i)}\cong\Gamma_2^{(j)}$. In Figs. 3(c) and 3(d), the distributions of H_i and $H_i+H_i(t)$ with $i=1$ and 2 calculated for each trajectory in the bundle are shown as functions of energy, which give the same information as the variances in Eq. (3.13). As is seen from Figs. 3(c) and 3(d), our numerical result well realizes the general inequality $0<\Gamma_1^{(1)}\cong\Gamma_1^{(2)}<\Gamma_2^{(1)}\cong\Gamma_2^{(2)}$. Namely, there are two kinds of width which tell us how two subsystems accommodate each other. It is also seen that the stationary state is established at $t\cong25\tau_{\rm coll}$, because the distribution of the partial energy has no strong time dependence after $t\cong25\tau_{\rm coll}$. This situation also coincides with the calculation in Fig. 2 and Figs. 3(a) and 3(b).

As is easily verified, the following relations also hold:

$$\langle H_\Delta^2\rangle_t-\langle H_\Delta\rangle_t^2=\langle H_{\rm mean}^2(t)\rangle_t-\langle H_{\rm mean}(t)\rangle_t^2\cong\Gamma_1^{(i)}, \tag{3.14}$$

$$\langle H_{\rm coupl}^2\rangle_t-\langle H_{\rm coupl}\rangle_t^2=\langle(H_1+H_2)^2\rangle_t-\langle H_1+H_2\rangle_t^2\cong\Gamma_2^{(i)}, \tag{3.15}$$

where $H_{\rm mean}(t)\equiv H_1+H_2+H_1(t)+H_2(t)$. From Eqs. (3.13), (3.14), and (3.15), one gets the relation

$$\langle H_\Delta^2\rangle_t-\langle H_\Delta\rangle_t^2\leqslant\langle H_{\rm coupl}^2\rangle_t-\langle H_{\rm coupl}\rangle_t^2. \tag{3.16}$$

The inequality relation (3.16) is well realized in our calculation which is illustrated in Fig. 3(e). In Fig. 3(f), the time dependence of the variance $\langle H_\Delta^2\rangle_t-\langle H_\Delta\rangle_t^2$ is shown. As is shown in Eq. (3.14) and is seen from Fig. 3(e), the variance $\langle H_{\rm mean}^2(t)\rangle_t-\langle H_{\rm mean}(t)\rangle_t^2$ has the same order of magnitude as $\Gamma_1^{(i)}$.

Since the square root of the variance $\langle H_\Delta^2\rangle_t-\langle H_\Delta\rangle_t^2$ is much larger than the $\langle H_\Delta\rangle_t$, which is understood by comparing Figs. 3(b) and 3(f), a large energy exchange goes on between the two subsystems, even though $\langle H_{i,\rm mean}(t)\rangle_t$ have reached the time-independent object, indicating no energy transfer in average. Namely, each subsystem cannot remain stationary alone by being separated from the other subsystem, when the following condition

$$\sqrt{\langle H_\Delta^2\rangle_t-\langle H_\Delta\rangle_t^2}>\langle H_\Delta\rangle_t=0 \tag{3.17}$$

holds, although the total system is in a statistical stationary state. In other words, the effect of $\rho_c(t)$ is so large that the total system cannot be divided into two subsystems when the relation (3.17) is valid.

C. Dynamic response function

In order to study what is happenning between two subsystems, let us use the dynamic response function which appears in the coupled master equation given below. By switching off the fluctuation $H_\Delta(t)$ between two subsystems at time t_I, and by evaluating its effects perturbatively in a small time increment after t_I, one gets a set of approximate coupled master equations given by

$$\begin{aligned}\dot\rho_1(t)=&-i[\mathscr{L}_1+\mathscr{L}_1(t)]\rho_1(t)-i{\rm Tr}_2P(t)\mathscr{L}g(t,t_I)\rho_c(t_I)\\&-\int_0^{t-t_I}d\tau\sum_{lm}\chi_{lm}(t,t-\tau)\{A^l,G_1(t,t-\tau)(A^m-\langle A^m\rangle_{t-\tau})\rho_1(t-\tau)\}_{\rm PB}\\&-\int_0^{t-t_I}d\tau\sum_{lm}\phi_{lm}(t,t-\tau)\{A^l,G_1(t,t-\tau)\{A^m,\rho_1(t-\tau)\}_{\rm PB}\}_{\rm PB},\end{aligned} \tag{3.18}$$

$$\begin{aligned}\dot\rho_2(t)=&-i[\mathscr{L}_2+\mathscr{L}_2(t)]\rho_2(t)-i{\rm Tr}_1P(t)\mathscr{L}g(t,t_I)\rho_c(t_I)\\&-\int_0^{t-t_I}d\tau\sum_{lm}\mathscr{X}_{lm}(t,t-\tau)\{B^l,G_2(t,t-\tau)(B^m-\langle B^m\rangle_{t-\tau})\rho_2(t-\tau)\}_{\rm PB}\\&-\int_0^{t-t_I}d\tau\sum_{lm}\Phi_{lm}(t,t-\tau)\{B^l,G_2(t,t-\tau)\{B^m,\rho_2(t-\tau)\}_{\rm PB}\}_{\rm PB},\end{aligned} \tag{3.19}$$

where the symbol $\{,\}_{\rm PB}$ denotes a Poisson bracket with respect to the canonical variables $(p_i,q_i,\ i=1$ and 2). In Eqs. (3.18) and (3.19), the fluctuation effects are retained up to the second order in $H_\Delta(t)$, and $g(t,t')$ represents a propagator

$$g(t,t')\equiv T\exp\left\{-i\int_t^{t'}[1-P(\tau)]\mathscr{L}d\tau\right\}. \qquad (3.20)$$

Approximate expressions in Eqs. (3.18) and (3.19) are good enough, provided the difference between the present time t and the switching-off time t_I is sufficiently small.

The functions $\chi_{lm}(t,t-\tau)$ and $\mathscr{X}_{lm}(t,t-\tau)$ appearing in Eqs. (3.18) and (3.19) are the *dynamic response functions*, whereas $\phi_{lm}(t,t-\tau)$ and $\Phi_{lm}(t,t-\tau)$ are the *dynamic correlation functions*. These are functions of two time arguments. The explicit expression of the dynamical response function is given by

$$\mathscr{X}_{kl}(t,t-\tau)\equiv\int\int dp_1dq_1\{G_1(t-\tau,t)A^k,A^l\}_{\rm PB}\rho_1(t-\tau),$$

$$\chi_{kl}(t,t-\tau)\equiv\int\int dp_2dq_2\{G_2(t-\tau,t)B^k,B^l\}_{\rm PB}\rho_2(t-\tau),$$

$$G_1(t,t')\equiv T\exp\left\{-i\int_{t'}^{t}d\tau[\mathscr{L}_1+\mathscr{L}_1(\tau)]\right\},$$

$$G_2(t,t')\equiv T\exp\left\{-i\int_{t'}^{t}d\tau[\mathscr{L}_2+\mathscr{L}_2(\tau)]\right\}, \qquad (3.21)$$

where $\mathscr{L}_1$, $\mathscr{L}_1(t)$, $\mathscr{L}_2$, and $\mathscr{L}_2(t)$, are the Liouvillian corresponding to H_1, $H_1(t)$, H_2, and $H_2(t)$, respectively.

As is clear from Eq. (3.21), the dynamical response function has two time arguments as compared to the ordinary linear response function. The latter has only one time argument, which measures how the subsystem deviates from the state of equilibration under the influence of an external force. The former contains another important information. Namely, it gives the instantaneous dynamical structure of the subsystems at the switching-off time $t_I\equiv t-\tau$, even though they are not in the statistical stationary state, and also how they evolve in time after t_I. It reduces to the conventional response function with only one time argument, which appears in the linear response theory applicable to the infinite system [see Eq. (4.5) and Ref. [7]], when the subsystems described by (q_1,p_1) and (q_2,p_2) reach their thermal equilibrium states. According to the numerical results discussed in the previous subsections, the statistical stationary state is expected to be established for the total system, when one takes $t_I\cong 20-25\tau_{\rm coll}$.

The numerical method of calculating the dynamic response function is found in our previous paper [5]. In Fig. 4, the dynamic response functions $\chi_{lm}(t_I+\tau,t_I)$ with $l=m=1$ (called collective) and with $l=m=2$ (called intrinsic) are shown as functions of τ for various t_I. These functions show how each subsystem responds to an "external" force coming from the coupling to the other subsystem and acting at the switching-off time t_I. Since they contain partial derivatives of H_Δ, small fluctuations in H_Δ give a drastic change in the dynamic response functions.

As is seen from Fig. 4, the collective and intrinsic dynamical response functions seem to reach stationary values around $t_I=(40–50)\tau_{\rm coll}$ which is much larger than $(20–25)\ \tau_{\rm coll}$. The difference between $(20–25)\tau_{\rm coll}$ and $t_I=(40-50)\tau_{\rm coll}$ is understood as follows: Although the variances in Fig. 2 seem to reach some stationary values, there still remains some small time dependence which can only be detected by their time derivatives. Since the dynamic response functions depend directly on the time derivatives of $\langle q_i^2\rangle_t-\langle q_i\rangle_t^2$ with $i=1$ and 2, the total system is considered to be in a stationary state when the dynamic response function has no t_I dependence. Strictly speaking, therefore, the stationary state for the total system is not established at $(20–25)\tau_{\rm coll}$, but around at $t=(40–50)\tau_{\rm coll}$.

Let us discuss the dynamic response function after $t_I=(40-50)\tau_{\rm coll}$. Since there is no t_I dependence in the dynamical response functions, the total system as well as its two subsystems already reached time-independent stationary objects. Note that each subsystem is only stationary under the influence of the other subsystem. As is seen from Fig. 4, these dynamic response functions show a remarkable property: They do not come back to their original value at t_I, unlike the case with the usual linear response function.

IV. RESPONSE FUNCTION FOR NONLINEAR COUPLING

In order to understand the remarkable feature of the dynamic response function shown in Fig. 4, let us introduce another simple model. The model consists of a harmonic oscillator with the coordinate q, mass M, and frequency ω_0, interacting with a heat bath. The heat bath consists of N harmonic oscillators described by coordinates x_i, frequencies ω_i, and the common mass m. The Hamiltonian is expressed as

$$H=H_S+H_B+H_I. \qquad (4.1)$$

Here,

$$H_S=\frac{p^2}{2M}+\frac{1}{2}M\omega_0^2q^2,$$

$$H_B=\sum_j\left(\frac{p_j^2}{2m}+\frac{1}{2}m\omega_j^2x_j^2\right). \qquad (4.2)$$

For the interaction H_I, we take two kinds of coupling: (a) linear coupling

$$H_I=q\sum_{j=1}^{N}\lambda_jx_j, \qquad (4.3)$$

which is applied in Ref. [16], and (b) nonlinear coupling

$$H_I=q\sum_{j=1}^{N}\lambda_jx_j^2. \qquad (4.4)$$

In order to study the behavior of the response function for the subsystem of the heat bath, which is coupled to the harmonic oscillator through the above two kinds of interaction, let us introduce the response function

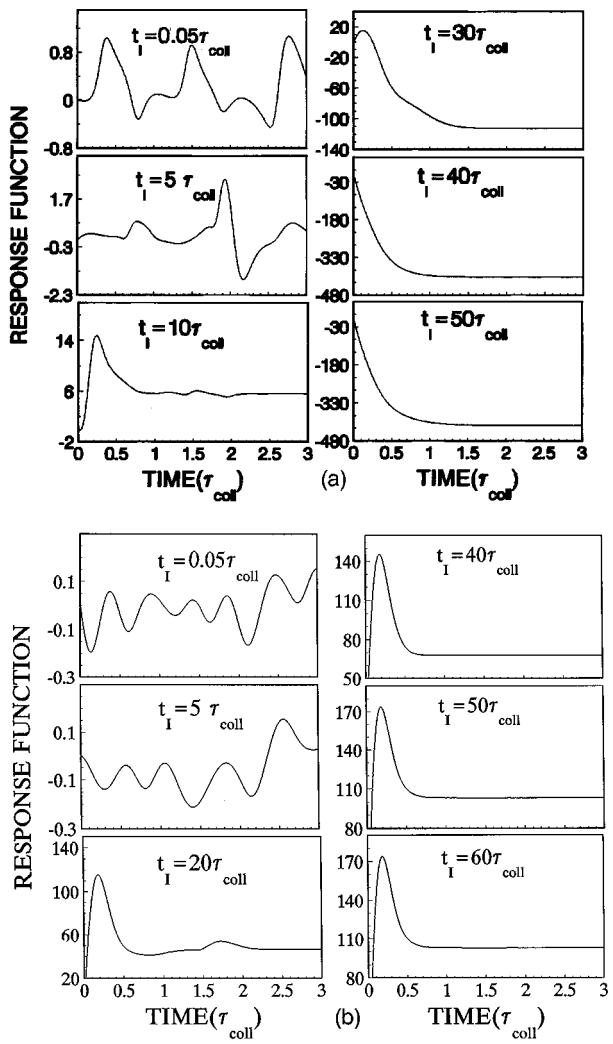

FIG. 4. (a) Dynamic response function with different switching times t_I for collective subsystem, and (b) for the intrinsic sybsystem, for the case with $V=-0.07$.

$$\chi(\tau)=\mathrm{Tr}_B\{G_{\mathrm{HB}}(\tau)B,B\}_{\mathrm{PB}}\rho_{\mathrm{HB}}. \tag{4.5}$$

Here, B denotes $B_{\mathrm{lin}}=\Sigma_{j=1}^{N}\lambda_j x_j$ for the linear coupling case, and $B_{\mathrm{non}}=\Sigma_{j=1}^{N}\lambda_j x_j^2$ for the nonlinear coupling case. $G_{\mathrm{HB}}(\tau)$ means a propagator of the heat bath and is expressed as

$$G_{\mathrm{HB}}(\tau)=\exp\{-i\tau\mathscr{L}\};\quad \mathscr{L}^*=\{H_B,^*\}_{\mathrm{PB}}. \tag{4.6}$$

For ρ_{HB}, we take the canonical ensemble with temperature T. The response function $\chi(\tau)$ then takes the form

$$\chi_{\mathrm{lin}}(\tau)=i\sum_{j=1}^{N}\lambda_j^2\frac{1}{m_j\omega_j}\sin\omega_j\tau,$$

$$\chi_{\mathrm{non}}(\tau)=i\sum_{j=1}^{N}\lambda_j^2\frac{1}{m_j^2\omega_j^2}\coth\frac{\omega_j}{2T}\sin2\omega_j\tau, \tag{4.7}$$

for the linear and the nonlinear coupling interactions, respectively. By introducing the Debye spectrum for the N harmonic oscillator system given by

$$\rho(\omega_j)=\frac{2\eta\omega_j^2 m_j}{\pi\lambda_j^2}, \tag{4.8}$$

the summation over j in Eq. (4.7) is replaced by an integral over frequency ω. Here, the parameter η is known to be related with the viscosity [16]. The response function is finally expressed as

$$\chi_{\mathrm{lin}}(\tau)=i\frac{2\eta}{\pi}\frac{1}{\tau}\left[\frac{\sin\Omega\tau}{\tau}-\Omega\cos\Omega\tau\right],$$

$$\chi_{\mathrm{non}}(\tau)=i\frac{2\eta}{\pi m}\int_0^{\Omega}\coth\frac{\omega}{2T}\sin2\omega\tau d\omega, \tag{4.9}$$

where Ω represents the upper limit of the Debye spectrum of the heat bath. In Fig. 5, the numerical results of $\chi_{\mathrm{lin}}(\tau)$ and $\chi_{\mathrm{non}}(\tau)$ are shown. The parameters used are $\eta=0.5$, $\Omega=100$, and $m=1$, and τ is expressed in units of τ_{coll}. As is seen from Eq. (4.9), $\chi_{\mathrm{lin}}(\tau)$ goes back to its original value of zero like the usual linear response function irrespective of the temperature T, when the time τ approaches infinity. However, $\chi_{\mathrm{non}}(\tau)$ describing the response to the nonlinear external force shows a quite similar feature to Fig. 4. By taking τ infinite, we get

$$\chi_{\mathrm{non}}(\tau\to\infty)=i\frac{2\eta}{m}\int_{-\Omega}^{\Omega}\omega\,\coth\frac{\omega}{2T}\delta(2\omega)d\omega=i\frac{2\eta T}{m}, \tag{4.10}$$

which obviously shows that the response of the thermal equilibrium state to a nonlinear external force does not come back to its original value, but converges to a constant value when the time approaches infinity. This remarkable feature is shown in Fig. 5(b) for three cases with different temperatures. By comparing Figs. 4 and 5, and by comparing B_{non} and B^i in Eq. (2.1), it is recognized that the specific feature of the dynamical response function at $t_I>(40\text{–}50)\tau_{\mathrm{coll}}$ is due to the nonlinear coupling to the other degrees of freedom. From this comparison, one may understand that the dynamical response function $\chi_{lm}(t_I+\tau,t_I)$ at $t_I>(40\text{–}50)\tau_{\mathrm{coll}}$ is effectively replaced by the response function for the nonlinear interaction, $\chi_{\mathrm{non}}(\tau)$, defined for the thermal equilibrium state. Since the effects of the rest subsystem appear only through the dynamical response and correlation functions, which is recognized from Eqs. (3.18) and (3.19), the possibility of the above replacement implies that the effects of the rest degrees of freedom on the subsystem under consideration are effectively expressed by the heat bath.

From the above discussion, one may draw the following conclusion: When the system with finite degrees of freedom reaches some statistical stationary state, and when the system is divided into two subsystems, the coupling to the other subsystem is effectively replaced by that to the heat bath.

V. SUMMARY

In order to study how the wave packet develops depending on its initial condition, the time evolution process of the bundle of trajectories initially located at a tiny unstable region (i.e., near the hypabolic point) of the TDHF manifold is studied within the TDHF theory. In this paper, we have stud-

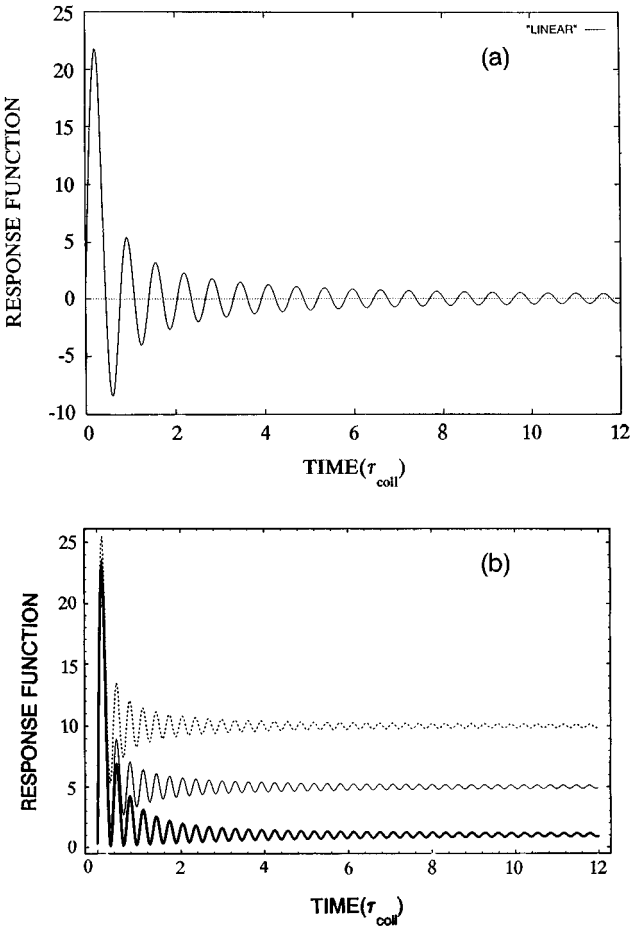

FIG. 5. (a) Response function for the heat bath with a linear coupling. (b) Response function for the heat bath with a nonlinear coupling. The thick solid, solid, and dashed curves are for $T=1$, 5, and 10, respectively.

ied how the strongly correlated system with finite degrees of freedom reaches its stationary state. By dividing the total system into two subsystems, the time development of the total system as well as the mutual dynamical interplay between two subsystems during the irreversible evolution process has been analyzed by means of the general theory of the coupled master equations. Even when the total system has reached some stationary statistical state, each subsystem cannot remain stationary by being separated from the other subsystem, when the square root of the variance $\langle H_\Delta^2\rangle_t - \langle H_\Delta\rangle_t^2$ is much larger than $\langle H_\Delta\rangle_t = 0$.

With the aid of the dynamic response functions, various dynamical states realized in the subsystem during the evolution process of the total system are discussed. When the total system reaches some stationary statistical state, as is clarified in Sec. III C, the dynamic response function of the subsystem shows a remarkable property which is different from the linear response function usually used in characterizing infinite condensed matter. It is shown that this specific property originates from the nonlinear coupling, and does not depend on the number of degrees of freedom of the subsystem or on the statistical assumption. Therefore, it is concluded that the concept of the temperature is justified microscopically even in a finite system with a few degrees of freedom. Since the response functions as well as the correlation functions are directly related to the experimental observables, the complex evolution process of finite many-body systems might be explored by means of these functions.

In this paper, we confined ourselves only to the simple two degrees of freedom problem where it is not possible to assign the collective degree of freedom or to discuss its dissipation. In deriving the Fokker-Planck- or Langevin-type transport equations microscopically, one needs more than three degrees of freedom. In this case, one can find a case where the total system is divided into two weakly coupled systems: One is composed of more than two degrees of freedom and is in a chaotic situation, and the other is near the regular motion almost sticking to the KAM torus. In such a case, the former can be effectively replaced by the heat bath as we learned from the present investigation, and the dissipation mechanism of the latter would be treated by the transport equation. These treatments, applied to the giant dipole resonance in the hot nuclei, are now in progress.

ACKNOWLEDGMENTS

We are grateful to K. Kumar for a careful reading of the manuscript. This work is supported in part by the National Natural Science Foundation of China and Foundation of Nuclear Science of China. Two of us (F.S. and Y.Z.) thank the Institute for Nuclear Theory at the University of Washington for its hospitality (INT Program ''Large Amplitude Collective Motion''), where the present work had been partially done.

[1] B.V. Chirikov, Phys. Rep. **52**, 263 (1979).
[2] A.J. Lichtenberg and M.A. Lieberman, *Regular and Stochastic Motion*, Applied Mathematical Science Vol. 38 (Springer, New York, 1983).
[3] Y. Zhuo and X. Wu, Chin. Phys. **1**, 969 (1981).
[4] F. Sakata, M. Matsuo, T. Marumori, and Y. Zhuo, Ann. Phys. (N.Y.) **194**, 30 (1989).
[5] X. Wu, F. Sakata, Y. Zhuo, and Z. Li, Phys. Rev. C **48**, 1183 (1993).
[6] F. Sakata and T. Marumori, *Direction in Chaos* (World Scientific, Singapore, 1992), Vol. 4, p. 459.
[7] R. Kubo, M. Toda, and N. Hashitsume, *Statistical Physics II*, Solid-State Science Vol. 31 (Springer, New York, 1985).
[8] H. Hofmann, in *Proceedings, Phase Space Approach to Nuclear Dynamics*, Trieste, 1985, edited by M. Di Toro, W. Nörenberg, M. Rosina, and S. Stringari (World Scientific, Singapore, 1986), p. 306 and references therein.
[9] W. Nörenberg, Phys. Lett. **104B**, 107 (1981).
[10] F. Barranco, R.A. Broglia, and G. Bertsch, Phys. Rev. Lett. **60**, 507 (1988).

[11] R.A. Broglia, F. Barranco, G.F. Bertsch, and E. Vigezzi, Phys. Rev. C **49**, 552 (1994).
[12] M. Matsuo, F. Sakata, and T. Marumori, Prog. Theor. Phys. **82**, 1084 (1989).
[13] F. Sakata, T. Kubo, T. Marumori, K. Iwasawa, and Y. Hashimoto, Phys. Rev. C **50**, 138 (1994).
[14] C.R. Willis and R.H. Picard, Phys. Rev. A **9**, 1343 (1974).
[15] O. Bohigas and M-J. Giannoni, *Chaotic Motion and Random Matrix Theories*, Lecture Notes in Physics Vol. 209 (Springer, New York, 1984), p. 1.
[16] A.C. Caldeia and A.J. Leggett, Ann. Phys. (N.Y.) **149**, 374 (1983); Physica **121A**, 587 (1983).